

Quantitative study on the cooling effect of green roofs in a high-density urban Area—A case study of Xiamen, China

Jing Dong ^a, Meixia Lin ^{b, c}, Jin Zuo ^{a, *}, Tao Lin ^{b, c, **}, Jiakun Liu ^d, Caige Sun ^e, Jiancheng Luo ^{c, f}

^a School of Architecture, Tianjin University, Tianjin, 300072, China

^b Key Laboratory of Urban Environment and Health, Institute of Urban Environment, Chinese Academy of Sciences, Xiamen, 361021, China

^c University of Chinese Academy of Sciences, Beijing, 100049, China

^d Department of Human Geography and Spatial Planning, Faculty of Geosciences, Utrecht University, Utrecht, 3584, CB, Netherlands

^e School of Geography, South China Normal University, Guangzhou, 510631, China

^f State Key Laboratory of Remote Sensing Science, Institute of Remote Sensing and Digital Earth, Chinese Academy of Sciences, Beijing, 100101, China



ARTICLE INFO

Article history:

Received 21 May 2019

Received in revised form

27 December 2019

Accepted 13 January 2020

Available online 23 January 2020

Handling editor: Jian Zuo

Keywords:

Green roofs

Cooling effect

High-density urban area

Urban heat island (UHI)

Remote sensing

Xiamen

ABSTRACT

Green roofs are thought to be an effective measure to solve the contradiction between land shortages and ecological construction, especially address urban heat island (UHI) effects in high-density urban areas. However, few empirical studies have focused on the cooling effect of green roof projects at urban scales. This study quantified the cooling effect of green roofs in Xiamen Island, China, where 540,000 m² of green roofs were implemented between 2015 and 2017, in order to address the two research questions: (1) do green roofs in high-density urban areas have a significant cooling effect at the city scale and (2) what is the extent of the cooling? The relative difference between the average land surface temperature (LST) of Xiamen Island and the green roofs stemmed from Landsat 8 remote sensing image in the summers of 2014 and 2017 were calculated in geographic information systems (GIS) to represent the cooling effect of green roof project. Results showed that: (1) the average LST difference between green roofs and Xiamen Island decreased by 0.91 °C, indicating that green roofs could effectively alleviate UHI effects in high-density urban areas; (2) The cooling effect was significant up to 100 m from the green roof installation in Xiamen Island, we called it as characteristic cooling buffer zone; (3) Regression analysis revealed that for every 1000 m² increase in green roof area, the average LST of the roof and its characteristic cooling buffer zone decreased by 0.4 °C. These findings provide the empirical proof for the cooling effect of green roofs on the surrounding environment in high-density urban areas and important insights for urban planners and government agencies for the effective mitigation of UHI impacts.

© 2020 Elsevier Ltd. All rights reserved.

1. Introduction

Urbanization and climate change are global concerns (Zhou, 2014; Santamouris et al., 2015). In 1950, urbanization averaged 30% globally. A period of rapid urbanization in the following 60 years (Li and Ye, 2015) resulted in the development of high-density

cities, which negatively influence urban spatial resources including land, energy, construction, and greening (Sung and Oh, 2011; Lin et al., 2016). Urbanization has also been found to aggravate the urban heat island (UHI) effect, which describes the phenomenon of higher temperatures in urban spaces relative to surrounding rural areas (Voogt and Oke, 2003; Peng et al., 2016; Zhou et al., 2017). A progressive increase in the UHI effect has been observed in both large cities and medium-sized municipalities (Barbieri et al., 2018). UHIs are a consequence of land use, urban morphology, climate conditions, anthropogenic heat emissions, and other factors (Sharma et al., 2017). Studies have shown that the underlying surface characteristics of urban areas have the most significant impact on UHIs (Shen et al., 2017). Furthermore, variations in daytime UHI intensity are more heavily influenced by the

* Corresponding author.

** Corresponding author. Key Laboratory of Urban Environment and Health, Institute of Urban Environment, Chinese Academy of Sciences, Xiamen, 361021, China.

E-mail addresses: 1198761187@qq.com (J. Dong), mxlin@iue.ac.cn (M. Lin), 8782606@qq.com (J. Zuo), tlin@iue.ac.cn (T. Lin), jkliu@iue.ac.cn (J. Liu), gecaisun@163.com (C. Sun), luojc@radi.ac.cn (J. Luo).

evaporative capacity of different land use types in wet areas (compared to arid areas). Thus, land use change is the driving factor of daytime UHI intensity (Li et al., 2019).

Negative impacts of UHIs include increased mortality (Norton et al., 2015), energy consumption, and air pollution; decreased comfort levels (Zhang et al., 2014); altered species composition and distribution (White et al., 2002); and increased ground-level ozone concentrations (Akbari et al., 2001). Consequently, the mitigation of UHI effects become an important research area in urban planning and ecology (Zhou et al., 2017; Amani-Beni et al., 2018). The cooling effects of green urban spaces have been widely documented (Zhang et al., 2014; Bowler et al., 2010; Kong et al., 2014). In high-density urban areas, demand for space and high land costs limit the provision of green space (Alex and Jim, 2012). Research has shown that green roofs are an effective strategy for mitigating UHI effects under limited land resources and planning strategies need to account for the comprehensive effects of green roofs on UHI (Santamouris, 2014; Luo et al., 2015; Teotónio et al., 2018; Sangkakool et al., 2018). However, lack of scientific understanding of these effects has been a primary obstacle for widespread implementation (Chun and Guldmann, 2014).

Extensive research has investigated the cooling effects of green space (Connors et al., 2013; Amani-Beni et al., 2019; Skelhorn et al., 2014), however, empirical studies examining the thermal profiles of green roofs and vertical greenery are limited (Koc et al., 2018). Current researches on cooling effect of green roofs can be classified into three categories: (a) observational, including on-site observations and remote sensing (Santamouris, 2014; Peng and Jim, 2015; Dos Santos et al., 2019); (b) statistical modelling and simulation (Shen et al., 2017; Chun and Guldmann, 2014; Smith and Roebber, 2011; Razzaghmanesh et al., 2016; Imran et al., 2018); and (c) experimental test (Koc et al., 2018; Razzaghmanesh et al., 2016). Field experiments indicate that all plant species result in significant green roof cooling (Cao et al., 2019). The daily maximum surface temperature of green roofs can be 10–30 °C lower as compared to conventional roofs (Santamouris, 2013; Yang et al., 2015) and simulations at the building and block scale have found benefits consistent with field experiments (Sailor et al., 2012; Zinzi and Agnoli, 2012). A recent observation study by Kohler and Kaiser (2019) show that the green roofs of some school buildings had a temperature stabilization effect of 1.5 K over a 20 year period.

In recent years, remote sensing has been widely used in UHI research because it can fully characterize the thermal environment of a city at a given time (Barbieri et al., 2018; Sun et al., 2013). Although the land surface temperature (LST) is not equal to the air temperature in the urban canopy layer, studies have confirmed that LST is highly correlated with near ground air temperature and is reliable to examine the relationship between UHIs and urban surface parameters (Voogt and Oke, 2003; Guo et al., 2019). To date, limited studies have researched the cooling effect of green roofs at a city scale because few urban regions have implemented sufficiently extensive green roofs to have a measurable impact beyond the building scale (Yang and Bou-Zeid, 2019). At this scale, numerical modelling, simulations, and statistical analysis have been used to predict different greening scenarios (Santamouris, 2014; Yang and Wang, 2017; Koc et al., 2018). Simulations have included atmospheric and urban canopy models, such as the Weather Research and Forecasting (WRF) model (Smith and Roebber, 2011; Yang and Bou-Zeid, 2019) and the WRF model coupled with the single Urban Canopy Model (Sharma et al., 2016). Santamouris (2014) reviewed simulations of green roof cooling, and found that implementation at the city level could decrease average ambient temperatures by 0.3–3 K. However, these simulations are pure theoretical and assumed that 100% of roofs were green, and considered roofs of extensive type (Georgescu et al., 2014; Sharma et al., 2016; Tewari

et al., 2019). Several studies have investigated partial green roof coverage. For example, Li et al. (2014) reported that more than 30% green or cool roof implementation reduced 2 m air temperatures by less than 0.2 °C. Yang and Bou-Zeid (2019) found that greening 25% of roofs reduced temperatures by up to 0.86 °C in city centers under favorable conditions. Imran et al. (2018) showed that the maximum surface UHI effect was reduced by 1–3.8 °C by increasing green roof fractions from 30 to 90%. Finally, Huang et al. (2019) found that 50% adoption of green roofs in an urban area decreased 2 m temperatures by 0.5 °C. Simulations that assume 100% green roof coverage cannot accurately assess the cooling effect of green roof projects at the city scale. Because most urban planning and design occurs at the city scale, this information is vital for local governments, developers, and practitioners (Koc et al., 2018). Furthermore, current research tend to focus on the cooling effect to green roof itself and pay little attention to the buffer zone around projects. A comprehensive assessment of how green roof installations affect temperatures at the city scale using observational data is vital to enable urban planners and governments to make feasibility decisions regarding green roof construction (Santos et al., 2016).

The objective of this study is to quantify the cooling effect based on real green roof projects in high-density urban areas at the city scale to address the following research questions: (1) do green roofs in high-density urban areas have a significant cooling effect at the city scale and (2) what is the extent of the cooling? In particular, we focus on the range of the effective cooling buffer zone (B_{CE}), and the quantitative relationship between green roof area and the LST of green roofs. To achieve this, Landsat 8 remote sensing image data from 2014 to 2017 were used with geographic information systems (GIS) to quantitatively analyze the cooling effect of urban green roofs.

2. Materials and methods

2.1. Survey area

Xiamen City, southeastern China, was chosen as the location for this study. Located between 24°23'–24°54' N and 117°53'–118°26' E, in the middle of the western bank of the Taiwan Strait, Xiamen is a sub-provincial city, a special economic zone, and an important scenic tourist city along China's southeastern coast (Fig. 1). Xiamen has a mild and rainy subtropical maritime monsoon climate. According to the Xiamen Statistical Yearbook, annual average temperature and rainfall are approximately 21 °C and 1200 mm, respectively. The rainy season lasts from May to August and the average wind speed is generally 2.7 m/s from the northeast. The research area of Xiamen Island is the urban center of Xiamen City with a land area of 142 km², and has gradually implemented green roofs since 2015. By 2017, the green roof area was 540,000 m², accounting for 2% of the entire urban rooftop area.

Xiamen Island was chosen as the location for this study because it represents a typical high-density urban area (Li et al., 2011). According to the Xiamen Statistical Yearbook, the built-up area of Xiamen increased by approximately 18 times in less than 30 years, and urbanization of the resident population is considered to be advanced stage (89% in 2017). A population density of more than 15,000 people/km² is the general threshold for high-density cities worldwide (Li and Ye, 2015), and Xiamen Island had a population density of 16,700 people/km² in 2017. The region is also ideally suited for this study because it experiences significant UHI effects. From 1994 to 2015, LST fluctuations in Xiamen City increased in severity. Land areas with low temperatures decreased continuously, while sub-high and high temperature areas increased, most notably after 2010. Among the administrative districts of Xiamen City, the warming trend in Xiamen Island is the most apparent, and

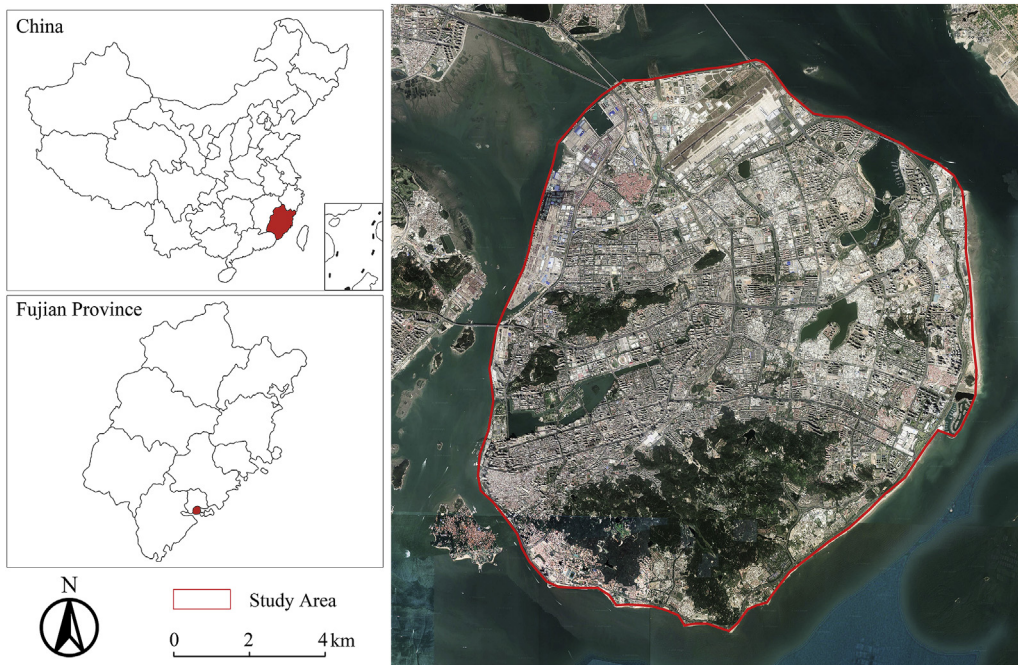


Fig. 1. Location map of Xiamen island in Fujian Province, China and the study area.

UHI effects are significant (Qin et al., 2018).

The 540,000 m² green roof space in 2017 was selected as the research object (Fig. 2). The roof space of the research object in 2014 (before green roof implementation) and 2017 (following green roof implementation) were used as control groups. Research objects also included a 30–500 m buffer zone surrounding the roofs. The minimum radius of the buffer zone was determined as the raster cell size of the remote sensing image (30 m) and the maximum radius was slightly larger than the biggest green roof diameter in study area (500 m) following Hamada and Ohta (2010) who found that the cooling effect of the urban park extended for several hundred meters. To study the gradient effect of the green roof cooling effect, multi-level buffer zones were generated according to the green roof boundary in increments of 30, 60, 90, 100, 120, 150, 180, 200, 300, 400, and 500 m in the GIS spatial analysis module. Thus, the 500 m buffer zone was divided into 11 sections (Fig. 3). By comparing LST changes in the different buffer zones, the cooling effect of the green roof was analyzed and the effective cooling area (B_{CE}) was selected as the characteristic cooling buffer zone for further quantitative analysis.

2.2. Data sources

Data on existing green roofs were collected by field investigation with collaboration of Xiamen municipal natural resources and planning bureau in 2017. To explore the cooling effects of green roofs in high-density urban areas, we used high-resolution remote sensing images to extract land use and LST data for Xiamen Island. Two years of data were used to represent before (2014) and after (2017) the implementation of green roofs. Landsat 8 remote sensing data (column number: 119043) were used to invert the LST. The data product downloaded from the geospatial data cloud was L1T, and the Landsat 8 thermal infrared band was resampled to 30 m resolution. Images were acquired on July 22, 2014 and October 02, 2017. Satellite transit time was approximately 10:33 a.m. (Beijing time) and the image data quality of the selected images was good, there was no cloud cover in the study area, and the atmospheric

visibility was high.

Landsat 8 carries an operational land imager (OLI) and thermal infrared sensor (TIRS). Band settings preserved all the band ranges of Landsat 7 ETM+, the narrow spectral ranges of some bands, and added the coast and cirrus bands. The thermal infrared band was increased from one ETM+ to two (Roy et al., 2014; Markham et al., 2014). Satellite parameters are shown in Table 1.

2.3. Methodology

Considering the dominant factors driving the UHI effect, the basic premise of this method is that land use changes on Xiamen Island between 2014 and 2017 are not significant, and roof space LST changes during this time stem from the implementation of green roofs. In existing research, the cooling effect of green infrastructure is generally quantified using the absolute value of single-phase LST (Barbieri et al., 2018; Amani-Beni et al., 2019; Guo et al., 2016, 2019). However, it is hard to identify the effect of green roofs in this way because average LST is a comprehensive result of various factors. In this study, we compared the relative difference between average LST. We calculated the average LST for Xiamen Island, the control group roofs, and their buffer zones before and after green roof implementation and compared the average LST difference between the control group roofs and Xiamen Island (ΔT_r), and the roof and its buffer zone (ΔT_b) as follows,

$$\Delta T_r = T_{rm} - T_{im} \quad (1)$$

$$\Delta T_b = T_{bm} - T_{rm} \quad (2)$$

where T_{rm} is the average LST of the control group roofs, T_{bm} is the average LST of the roof buffer zone, and T_{im} is the average LST for Xiamen Island.

We assume that LST increases significantly with ΔT_b . As buffer zone distance increases, the LST change curve will eventually flatten or begin to go down, indicating that the cooling effect is no longer apparent. Therefore, the intersection of the 2014 and 2017

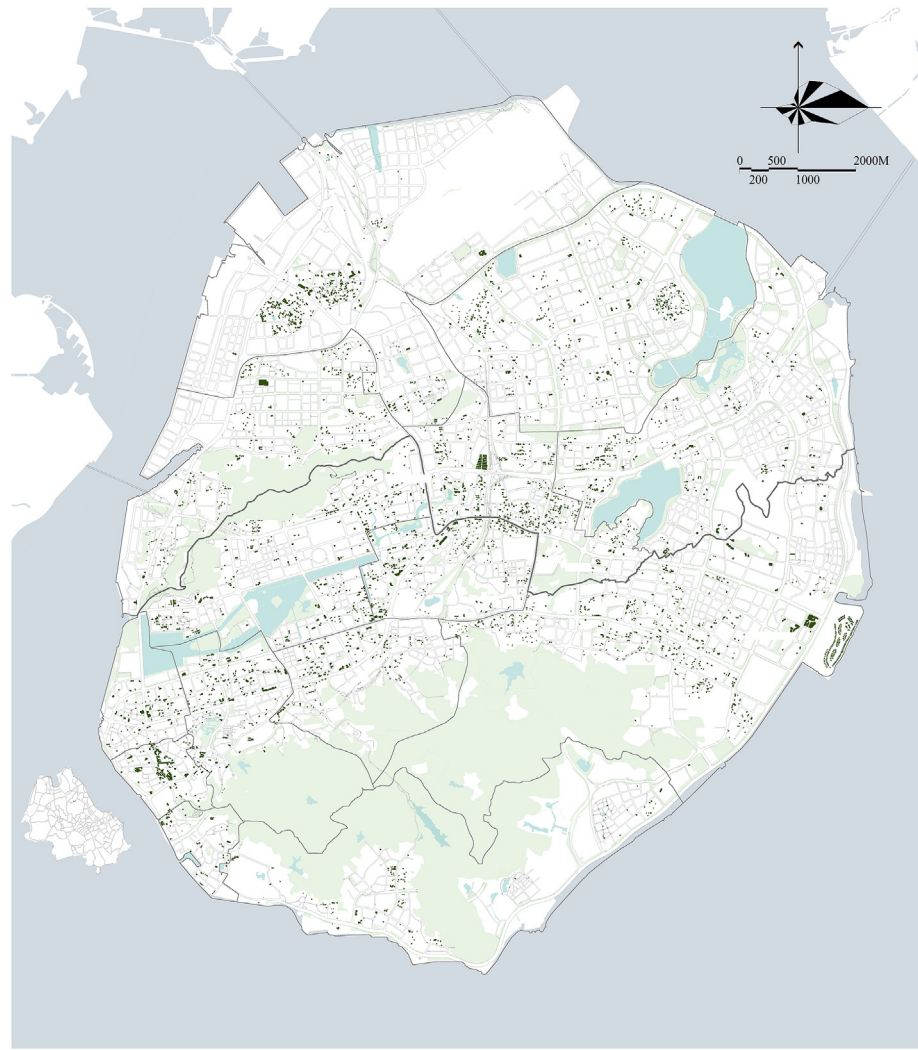


Fig. 2. The space layout of green roofs. (For interpretation of the references to colour in this figure legend, the reader is referred to the Web version of this article.)

LST curves indicates the extent of green roof influence on the surrounding thermal environment, defined herein as the characteristic cooling buffer zone (B_{CE}).

Fig. 4 shows a flowchart of the methodology used in this study. Firstly, land use information was interpreted and classified and the LSTs of Xiamen Island before and after green roof implementation were obtained. Secondly, the LST difference between Xiamen Island and the control group roofs and the control group roofs and their buffer zones were calculated. Then, the B_{CE} was determined by comparing cooling in different buffer zones. Finally, the relationship between green roof area, average LST of roof and B_{CE} were quantified using regression analysis.

2.3.1. Land use type

The vegetation index method was used to extract green space information. The normalized difference vegetation index (NDVI) represents vegetation cover on the land surface as follows (Santamouris et al., 2015):

$$\text{NDVI} = \frac{B_{NIR} - B_R}{B_{NIR} + B_R} \quad (3)$$

where B_{NIR} and B_R represent the reflection values of the near-infrared band and red band, respectively. For Landsat 8, the

fourth and fifth bands are the red and near-infrared bands, respectively.

Vegetation coverage information can be extracted by calculating NDVI and establishing a threshold based on empirical data and actual conditions. The NDVI threshold method was used to divide the urban surface of Xiamen Island into three types: built-up area ($0 \leq \text{NDVI} \leq \text{threshold}$), green land ($\text{NDVI} > \text{threshold}$) and water ($\text{NDVI} < 0$). The NDVI thresholds were 0.4 in 2014 and 0.3 in 2017. Then, post-classification was used to improve classification accuracy. Finally, random sampling (20 samples of each type) was used to evaluate the accuracy of the classification results. Kappa coefficients in both 2014 and 2017 were greater than 0.8, indicating that the land use classification results were acceptable.

2.3.2. Land surface temperature (LST)

Landsat 8 OLI-TIRS data has two thermal infrared bands; however, we used band 10 to determine LST due to uncertainties with band 11. Considering the influence of the atmosphere and surface on temperature, we adopted a mono-window algorithm (Qin et al., 2001) based on the heat radiation conduction equation to invert LST. There are four main parameters in LST retrieval: land surface brightness temperature, average atmospheric temperature, atmospheric transmittance, and land surface emissivity.

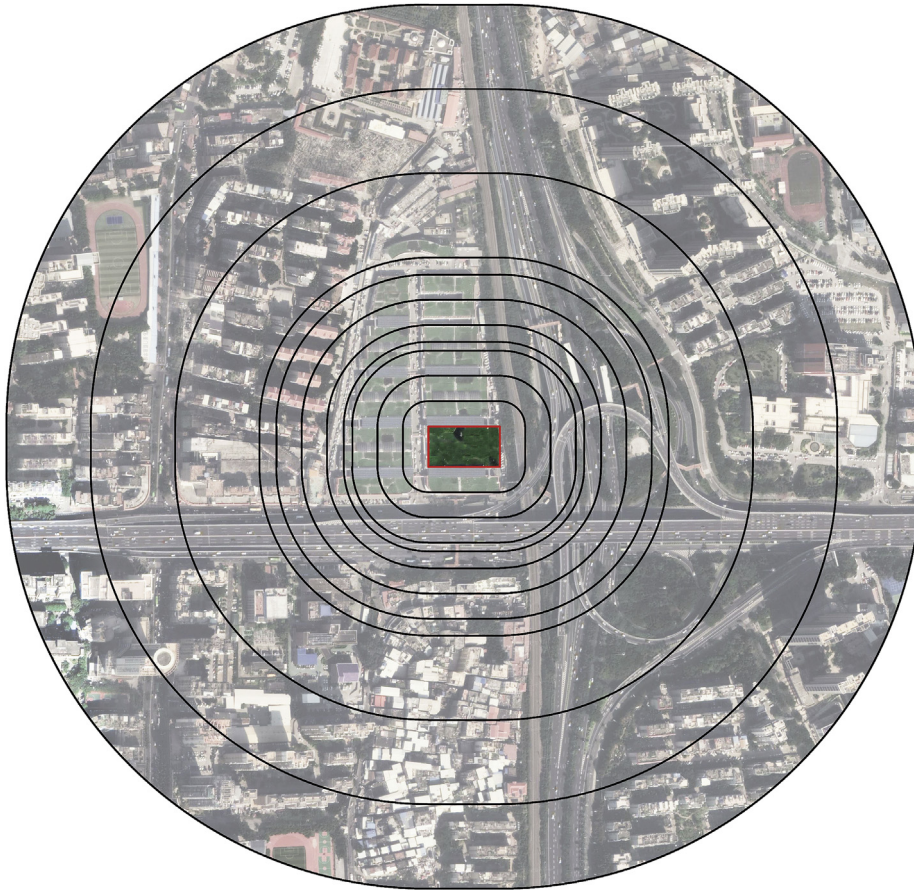


Fig. 3. Sketch map of roof buffer zone.

2.3.2.1. Land surface brightness temperature. Land surface brightness temperature refers to the temperature corresponding to the thermal radiation intensity observed by satellite. It is usually lower than the actual temperature, also known as the surface radiation temperature and is determined as follows:

$$L_\lambda = DN \times \frac{L_{max} - L_{min}}{255} + L_{min} \quad (4)$$

$$T_b = \frac{K_2}{\ln\left(\frac{K_1}{L_\lambda} + 1\right)} \quad (5)$$

where L_λ is the thermal radiation intensity, T_b is the land surface

brightness temperature of band 10, DN represents the gray value of the thermal infrared band (band 10), L_{min} and L_{max} are the minimum and maximum radiances detected by the sensor, and K_1 and K_2 are constants. For Landsat 8, $K_1 = 774.89 \text{ mW} \cdot \text{cm}^{-2} \cdot \text{sr}^{-1} \cdot \mu\text{m}^{-1}$ and $K_2 = 1321.08 \text{ K}$.

2.3.2.2. Land surface emissivity. Methods for estimating land surface emissivity (ϵ) include: (a) a mathematical relationship using parameters manually obtained with a thermal infrared spectrometer; (b) calculating the specific emissivity of the black body under ideal conditions and estimating ϵ using relevant parameters based on specific data; and (c) a functional relationship between surface emissivity and NDVI. According to this functional relationship and vegetation coverage (F; calculated based on NDVI), land surface

Table 1
Landsat 8 satellite parameters.

Sensor	Band number	Name	Wavelength (μm)	Spatial resolution (m)	Radiometric resolution (bit)
OLI	1	Coastal	0.43–0.45	30	12
	2	Blue	0.45–0.52	30	12
	3	Green	0.53–0.60	30	12
	4	Red	0.63–0.68	30	12
	5	NIR	0.85–0.89	30	12
	6	SWIR 1	1.56–1.66	30	12
	7	SWIR 2	2.10–2.30	30	12
	8	Pan	0.50–0.68	15	12
	9	Cirrus	1.36–1.39	30	12
TIRS	10	TIRS 1	10.60–11.20	100	12
	11	TIRS 2	11.50–12.50	100	12

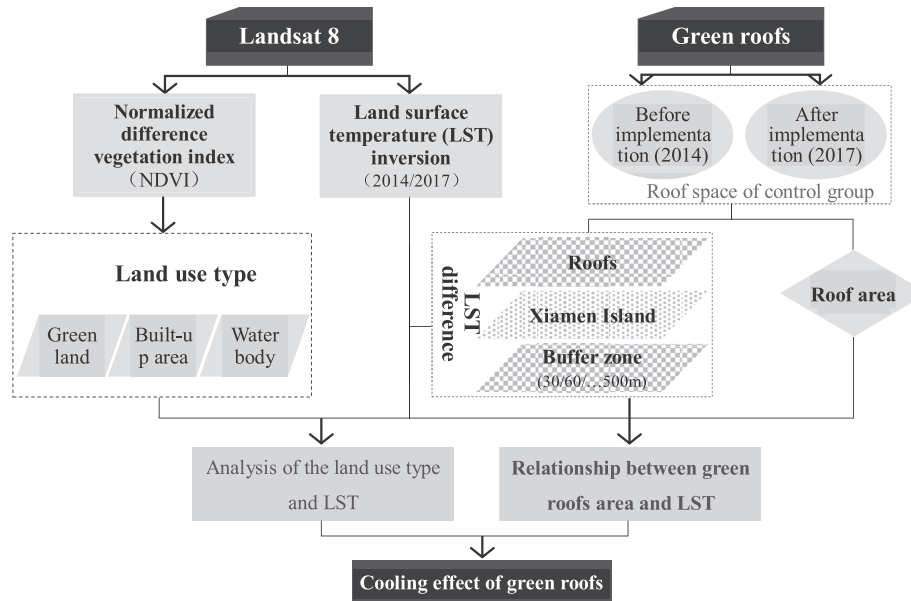


Fig. 4. A technique flowchart of the methodology applied in the present analysis.

Table 2

Linear relationship between atmospheric mean temperature and LST.

Applicable area	Model
US 1976 average atmosphere	$T_a = 25.9396 + 0.88045T_0$
Tropical average atmosphere	$T_a = 17.9769 + 0.91715T_0$
Mid-latitude winter average atmosphere	$T_a = 19.2740 + 0.91118T_0$
Mid-latitude summer average atmosphere	$T_a = 16.0110 + 0.92621T_0$

emissivity can be estimated as follows (Zribi et al., 2003):

$$\epsilon = 0.004F + 0.986 \quad (6)$$

2.3.2.3. Average atmospheric temperature. Average atmospheric temperature (T_a) can be difficult to obtain. Previous studies have found that the average atmospheric temperature has a linear relationship with 2 m temperatures (T_0). Qin et al. (2001) simulated the relationship between T_0 and T_a under standard atmospheric conditions and without actual atmospheric profile data, as shown in Table 2.

Based on the location of Xiamen City and data acquisition time, the mid-latitude summer average atmospheric model was used to calculate the average atmospheric temperature, according to Table 2. The units of T_0 and T_a are both K, which can be converted to t with a unit of $^{\circ}\text{C}$.

2.3.2.4. Atmospheric transmittance. The atmospheric transmittance (τ) is the ratio of radiation intensity passing through the atmosphere to radiation intensity before incidence. It is difficult to calculate τ due to many influencing factors, however, reliable τ can be obtained from the National Aeronautics and Space Administration official website which provides the atmospheric transmittance after 2000, including imaging time and central latitude and longitude.

2.3.2.5. Land surface temperature. The LST was inverted based on the mono-window algorithm model as follows:

$$C = \epsilon\tau \quad (7)$$

$$D = (1 - \epsilon)[1 + (1 - \epsilon)\tau] \quad (8)$$

$$LST = \frac{a(1 - C - D) + [b(1 - C - D) + C + D] \times T_b + D \times T_a}{C} \quad (9)$$

where a and b are constants (when the temperature is between 0 and 70°C , $a = -67.3554$ and $b = 0.458$) and C and D are intermediate variables related to surface emissivity and atmospheric transmittance.

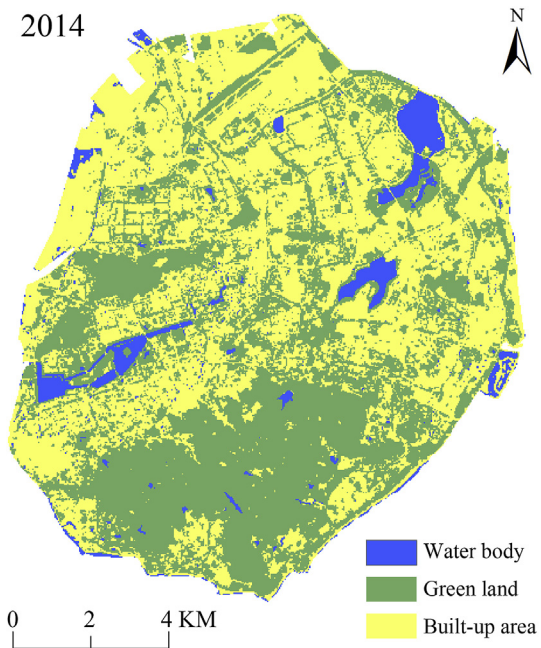
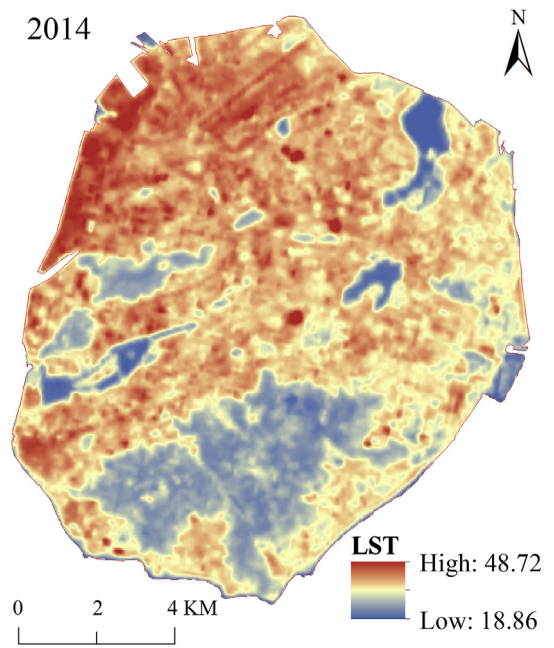
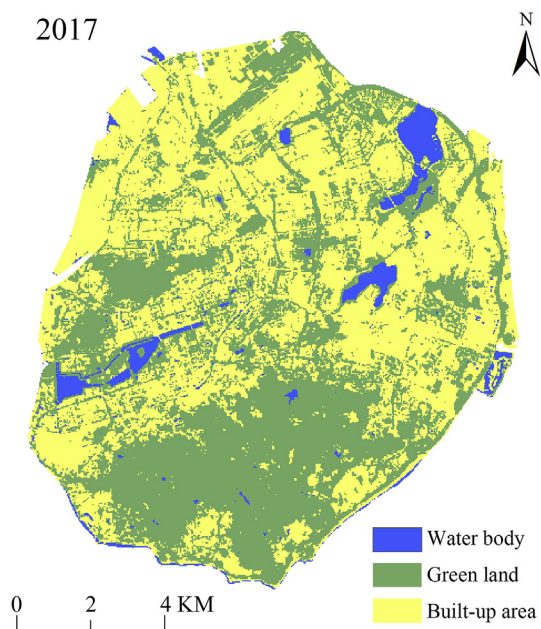
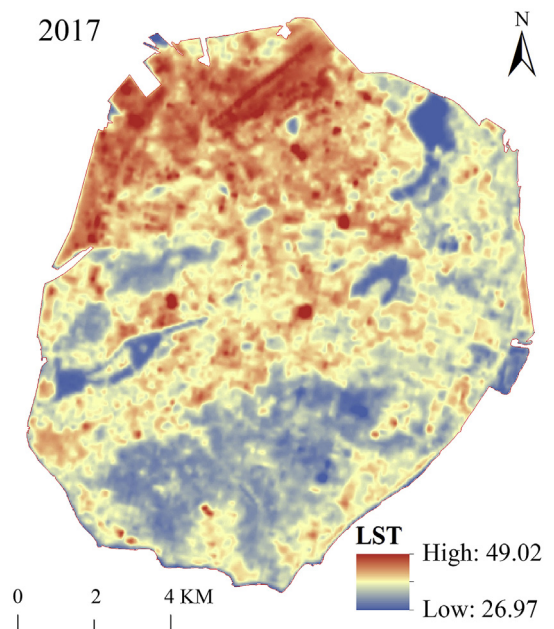
2.3.3. Statistical analysis

SPSS software was used for paired t tests and Spearman correlation analysis. Paired t tests were conducted on 4,436 data pairs. Theoretically, Spearman correlation analysis is used to represent the direction and degree of change trend between two variables, and its value (Spearman correlation coefficient) ranges from -1 to $+1$. Zero means that the two variables are not correlated. A positive (negative) value indicates positive (negative) correlation. A larger coefficient indicates a stronger correlation. Using a single roof as the research object, Spearman correlation analysis was used to examine the correlation between the average LST of green roofs and their characteristic cooling buffer zone with green roof area. On this basis, regression analysis was conducted to explore the quantitative relationship between the green roof area and the average LST of the roof and buffer zone.

3. Results and discussion

3.1. Landscape pattern and LST

Figs. 5 and 6 show the results of land use classification. The spatial landscape of Xiamen Island did not change markedly between 2014 and 2017 especially the landscape pattern around the urban built-up area. The built-up area of Xiamen Island in 2017 was only 0.18 km^2 larger as compared to 2014, while water and green land areas decreased by 1.03 km^2 and increased by 0.75 km^2 ,

**Fig. 5.** Land use map of Xiamen Island in 2014.**Fig. 7.** LST of Xiamen island in 2014.**Fig. 6.** Land use map of Xiamen Island in 2017.**Fig. 8.** LST of Xiamen island in 2017.**Table 3**

Statistics of land use and LST changes of Xiamen Island in 2014 and 2017.

	Land use area (km^2)			Average LST ($^{\circ}\text{C}$)		
	Water body	Built-up area	Green land	Xiamen Island	Green roofs	ΔT_r
2014	6.57	62.75	73.35	31.96	33.13	1.17
2017	5.54	62.93	74.1	36.5	36.76	0.26
Difference	-1.03	0.18	0.75	4.54	3.63	-0.91

 ΔT_r = Average LST of green roofs - Average LST of Xiamen Island.

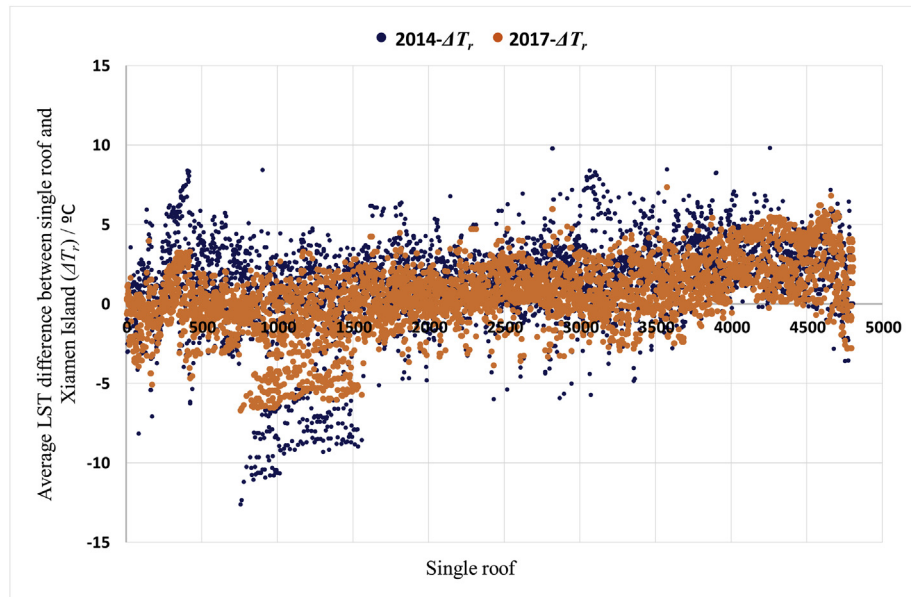


Fig. 9. Scatter plots of average LST difference between single roof and Xiamen Island (ΔT_r) in 2014 and 2017.

respectively (Table 3). Figs. 7 and 8 show that the spatial distribution of LST in Xiamen Island did not change markedly either between 2014 and 2017. Low temperature areas were mainly concentrated in the south and high temperature areas were mainly distributed in the north. The most severe UHI effect was in the northwest. Compared to 2014, the average LST of Xiamen Island increased by 4.54 °C in 2017, and green roof area increased by 3.63 °C.

3.2. LST and green roofs

LST results for 2014 and 2017 (Table 3) show that prior to the implementation of green roofs, the average LST of Xiamen Island and the green roofs were 31.96 °C and 33.13 °C, respectively. Following green roof implementation, the average LST of Xiamen Island and the green roofs were 36.50 °C and 36.76 °C, respectively. Following green roof implementation, the average LST difference between the green roofs and Xiamen Island decreased by 0.91 °C.

This result is consistent with previous studies which showed that green roofs decreased average ambient temperatures between 0.3 and 3 K at the city scale (Santamouris, 2014; Huang et al., 2019; Imran et al., 2018; Yang and Bou-Zeid, 2019). Paired t-test results (Fig. 9) show that there was a general cooling effect on roofs following green roof implementation ($n = 4435$, $p < 0.01$), suggesting that the green roofs in the high-density urban area are helping to mitigate UHI effects on Xiamen Island.

3.3. Quantitative analysis

3.3.1. Characteristic cooling buffer zone (B_{CE})

Fig. 10 shows the LST difference between the roof and its buffer zone (ΔT_b) pre and post green roof implementation. Within the 30–100 m buffer zone, ΔT_b was smaller following green roof implementation. While within the 100–150 m buffer zone, the ΔT_b was larger following green roof implementation. That means the implementation of green roof narrows the temperature difference

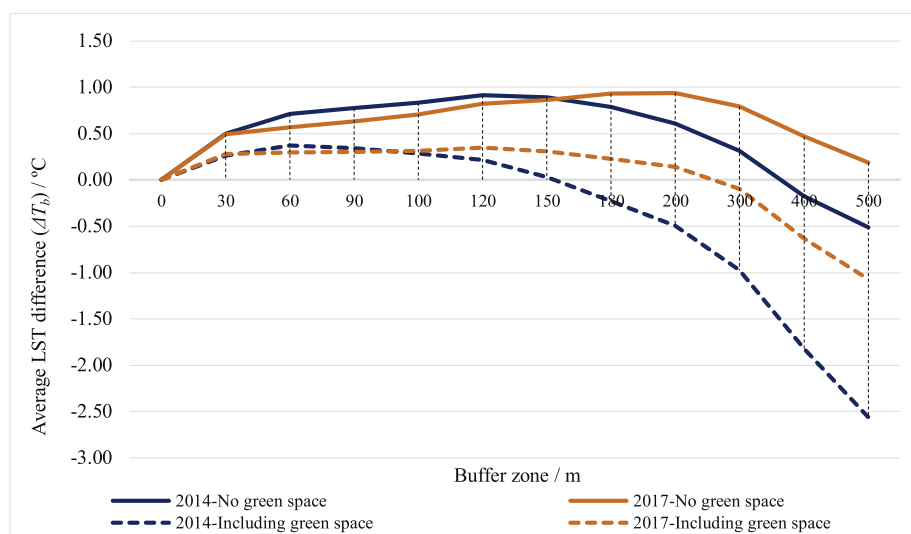


Fig. 10. Change chart of average LST difference between green roofs and multistage buffer ring in 2014 and 2017 (ΔT_b)/°C. (For interpretation of the references to colour in this figure legend, the reader is referred to the Web version of this article.)

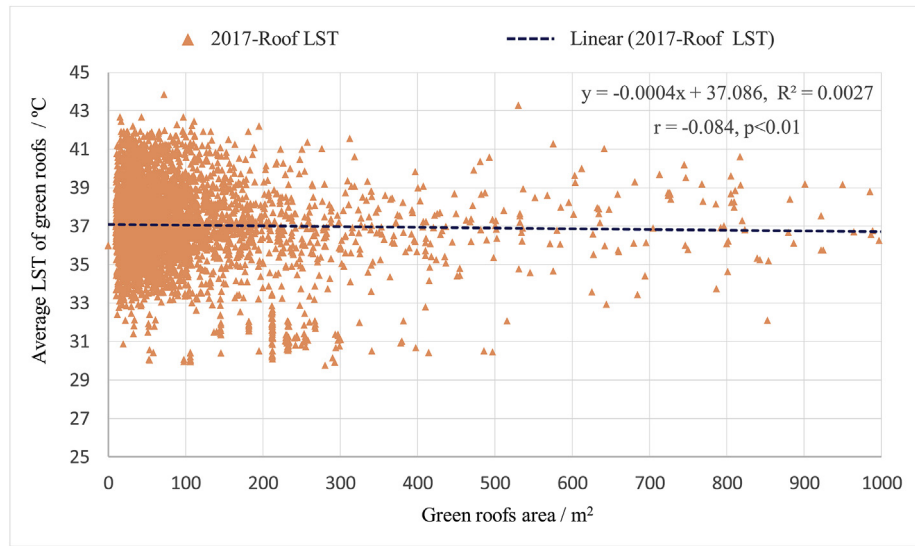


Fig. 11. Relationship between average LST of green roofs and green roofs area. (For interpretation of the references to colour in this figure legend, the reader is referred to the Web version of this article.)

between green roof and its surroundings, i.e., green roof may have a cooling effect in some distance, but we cannot exclude the influence of green space around the green roof. Most previous studies have demonstrated that green space is a kind of cooling island itself. Average LST of green space is lower than that of its surroundings (Amani-Beni et al., 2019; Guo et al., 2019). To eliminate the influence of green space in the buffer zone, areas of green space were removed (water areas were negligible), and ΔT_b was recalculated at each buffer zone (shown by the solid line in Fig. 10). After the removal of green space, ΔT_b also had a tendency to be smaller following green roof implementation within the 30–150 m buffer zone. Therefore, this supplementary experiment demonstrates that green space in buffer zone strengthens the cooling island effect on its surroundings, which makes the average LST of buffer zones lower ($\Delta T_b = T_{bm} - T_{rm}$, T_{rm} is the average LST of green roof and keeps unchanged, dash line is always below the solid line within 150m where $\Delta T_b \geq 0$).

Based on these findings, although excluding the influence of green space itself made maximum cooling range of Xiamen Island

green roofs to surrounding environment extend from 100m to 150 m, we still cannot ignore the cooling island effect of green space on its surroundings. Consider that, we choose the minimum distance (100m) as the characteristic cooling buffer zone (B_{CE}) of green roofs. Previous studies have found that land use types and urban morphology (Guo et al., 2016; Maggiotto et al., 2014; Coseo and Larsen, 2014) have a marked impact on LST changes. Furthermore, under higher temperatures and lower relative humidity, the cooling effect of green vegetation is more significant (Perini and Magliocco, 2014). Therefore, in cities with different climatic conditions and spatial characteristics, the B_{CE} of green roofs may differ, and green roof projects should be planned based on the B_{CE} of the target city.

3.3.2. Relationship between green roof area and cooling

Using a single roof as a research sample, spearman statistical analysis was used to analyze the correlation between green roof area and average LST of green roofs and B_{CE} (within 100 m buffer zone; Figs. 11 and 12). Results show that both LST of green roofs

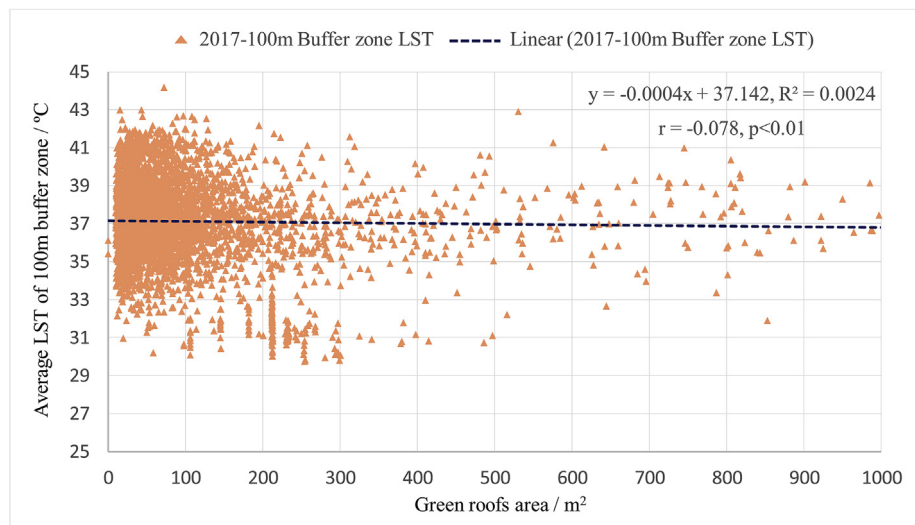


Fig. 12. Relationship between average LST of 100 m buffer zone and green roofs area. (For interpretation of the references to colour in this figure legend, the reader is referred to the Web version of this article.)

Table 4

The curve regression of LST and green roof area.

	Regression models	R ²	P-value
LST of green roofs and green roof area	Linear	0.0027	0.001
	Logarithmic	0.0140	0.000
	Inverse	0.0001	0.584
	Quadratic	0.0035	0.000
	Cubic	0.0099	0.000
	Compound	0.0031	0.000
	Power	0.0160	0.000
	S	0.0001	0.612
	Growth	0.0031	0.000
	Exponential	0.0031	0.000
	Logistic	0.0031	0.000
LST of B_{CE} and green roof area	Linear	0.0024	0.001
	Logarithmic	0.0152	0.000
	Inverse	0.0002	0.399
	Quadratic	0.0039	0.000
	Cubic	0.0104	0.000
	Compound	0.0027	0.000
	Power	0.0173	0.000
	S	0.0001	0.419
	Growth	0.0027	0.000
	Exponential	0.0027	0.000
	Logistic	0.0027	0.000

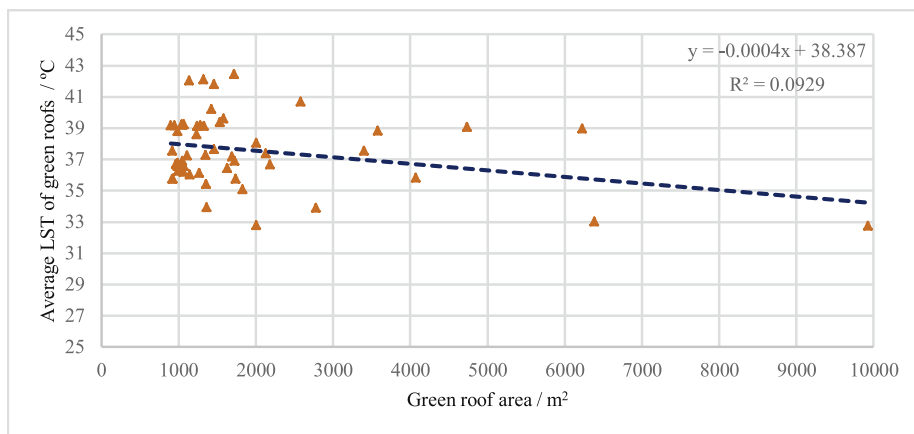


Fig. 13. The linear fitting and regression of LST of green roofs and green roof area $\geq 900 \text{ m}^2$. (For interpretation of the references to colour in this figure legend, the reader is referred to the Web version of this article.)

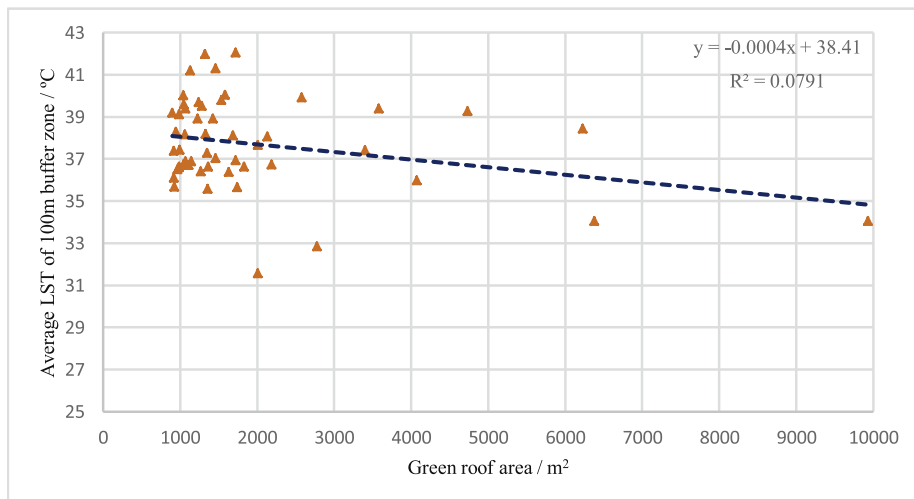


Fig. 14. The linear fitting and regression of LST of 100 m buffer zone and green roof area $\geq 900 \text{ m}^2$. (For interpretation of the references to colour in this figure legend, the reader is referred to the Web version of this article.)

(-0.084 , $p < 0.01$) and B_{CE} (-0.078 , $p < 0.01$) were negatively correlated with green roof area when the biggest roof area did not exceed $10,000 \text{ m}^2$, indicating that the cooling effect was stronger as green roof area increased. Using linear fitting and regression analysis, the linear regression equation of LST of green roofs and green roof area is $Y = -4 \times 10^{-4}x + 37.086$, and LST of B_{CE} and green roof area is $Y = -4 \times 10^{-4}x + 37.142$. The coefficient of determination (R^2) of the regression for the LST and the green roof area in Xiamen Island were all relatively small (Table 4). The possible reason maybe that our study did not consider the impact of factors such as scattered samples, landscape configuration around green roofs, and urban surface morphology. Since our research mainly focuses on the quantitative relationship between green roof area and the LST of green roofs, other regression models cannot obtain a fixed slope (the slope represents the cooling value), i.e., quantitative results of green roof area and cooling value cannot be obtained, and the linear regression is more stable. We selected the green roof samples with area $\geq 900 \text{ m}^2$ which are more reliable from remote sensing and fitted them with linear regression. The coefficient of determination (R^2) was slightly improved, and the slope of the function remained as -4×10^{-4} (Figs. 13 and 14). In summary, the average LST of green roofs and B_{CE} in high-density urban areas can be reduced by 0.4°C for every 1000 m^2 increase in green roof space.

Besides, our study analyzed the cooling effect of green roofs by comparing ΔT_r and ΔT_b before and after implementation. Because green roofs reduced the average LST of Xiamen Island, our method may underestimate the cooling effect to some extent. This also means that, with increased green roof coverage in the future, the relative LST difference between Xiamen Island and green roof may be smaller.

4. Conclusions

In recent years, green roofs are thought to be an effective means of resolving the conflict between land shortage and ecological construction to alleviate UHI effects in high-density urban areas. It is important to quantify the impact of green roofs on UHIs. Previous studies have demonstrated the performance and benefits of green roofs in laboratory conditions or at small scales. However, few empirical studies confirm the cooling effect of green roof projects at the city scale. Using Landsat 8 remote sensing image data with GIS, this study quantified the cooling effect of urban green roofs on Xiamen Island for the summers of 2014 and 2017, which represented the pre and post implementation phases of the green roof project of $540,000 \text{ m}^2$ that covered 2% of the entire urban rooftop area. Our findings showed that green roofs had a significant impact on the LST surrounding the green roof and could effectively regulate the thermal environment of high-density urban areas. The average LST difference between green roof areas and Xiamen Island was reduced by 0.91°C because of the green roof and the green roof cooling effect was significant within a radius of 100 m. The LST of roofs and 100m buffer zone were negatively correlated with green roof area. The LST of green roofs and 100m buffer zone in high-density urban areas were reduced by 0.4°C for every 1000 m^2 increase in green roof space. These findings demonstrate that green roofs are an effective strategy to alleviate UHI effects. Determining the cooling effects of green roofs requires long-term observations. Future research should combine seasonal data to comprehensively understand the mechanisms driving the cooling effects of green roofs. Our study was conducted in the context of a coastal city with a subtropical monsoon climate, and results may vary under different climate conditions. Our study provides useful insights into the quantitative relationship between LST and green roofs using the actual green roof project implemented at the city scale. Future studies should include similar analysis in other cities, as the results

appear sensitive to local conditions. On the other hand, whether the cooling effect of green roofs will match the expectations of UHI mitigation strategies depends on both the spatial configuration and scale of green roof implementation. Therefore, mitigation strategies should be designed based on the characteristics of individual cities, especially with respect to the green roof cooling buffer. The findings of this study provide a baseline for further study regarding how to maximize the cooling effect of green roofs.

Declaration of competing interest

The authors declare that they have no known competing financial interests or personal relationships that could have appeared to influence the work reported in this paper.

CRediT authorship contribution statement

Jing Dong: Writing - original draft, Writing - review & editing, Visualization, Investigation, Formal analysis. **Meixia Lin:** Software, Methodology, Data curation, Investigation, Writing - review & editing. **Jin Zuo:** Conceptualization, Validation, Supervision, Resources, Project administration, Funding acquisition. **Tao Lin:** Methodology, Supervision, Validation, Writing - review & editing. **Jiakun Liu:** Software, Data curation. **Caige Sun:** Software, Data curation. **Jiancheng Luo:** Data curation, Formal analysis.

Acknowledgments

This work was supported by the National Key Research and Development Program of China [2016YFC0502903].

References

- Akbari, H., Pomerantz, M., Taha, H., 2001. Cool surfaces and shade trees to reduce energy use and improve air quality in urban areas. *Sol. Energy* 70, 295–310. [https://doi.org/10.1016/S0038-092X\(00\)00089-X](https://doi.org/10.1016/S0038-092X(00)00089-X).
- Alex, Y.H.L., Jim, C.Y., 2012. Citizen attitude and expectation towards greenspace provision in compact urban milieus. *Land Use Policy* 29, 577–586. <https://doi.org/10.1016/j.landusepol.2011.09.011>.
- Amani-Beni, M., Zhang, B., Xie, G., Xu, J., 2018. Impact of urban park's tree, grass and waterbody on microclimate in hot summer days: a case study of Olympic Park in Beijing, China. *Urban For. Urban Green.* 32, 1–6. <https://doi.org/10.1016/j.ufug.2018.03.016>.
- Amani-Beni, M., Zhang, B., Xie, G.D., Shi, Y., 2019. Impacts of urban green landscape patterns on land surface temperature: evidence from the adjacent area of Olympic Forest Park of Beijing, China. *Sustainability* 11, 513. <https://doi.org/10.3390/su11020513>.
- Barbieri, T., Despini, F., Teggi, S., 2018. A multi-temporal analyses of land surface temperature using landsat-8 data and open source software: the case study of Modena, Italy. *Sustainability* 10, 1678. <https://doi.org/10.3390/su10051678>.
- Bowler, D.E., Buyung-Ali, L., Knight, T.M., Pullin, A.S., 2010. Urban greening to cool towns and cities: a systematic review of the empirical evidence. *Landscape Urban Plan.* 97, 147–155. <https://doi.org/10.1016/j.landurbplan.2010.05.006>.
- Cao, J.J., Hu, S., Dong, Q., Liu, L.J., Wang, Z., 2019. Green roof cooling contributed by C3, C4, and CAM Plant species. *Energy Build.* 195, 45–50. <https://doi.org/10.1016/j.enbuild.2019.04.046>.
- Chun, B., Guldmann, J.M., 2014. Spatial statistical analysis and simulation of the urban heat island in high-density central cities. *Landscape Urban Plan.* 125, 76–88. <https://doi.org/10.1016/j.landurbplan.2014.01.016>.
- Connors, J.P., Galletti, C.S., Chow, W.T.L., 2013. Landscape configuration and urban heat island effects: assessing the relationship between landscape characteristics and land surface temperature in Phoenix, Arizona. *Landscape Ecol.* 28, 271–283. <https://doi.org/10.1007/s10980-012-9833-1>.
- Coseo, P., Larsen, L., 2014. How factors of land use/land cover, building configuration, and adjacent heat sources and sinks explain urban heat islands in Chicago. *Landscape Urban Plan.* 125, 117–129. <https://doi.org/10.1016/j.landurbplan.2014.02.019>.
- Dos Santos, S.M., Silva, J.F.F., Dos Santos, G.C., De Macedo, P.M.T., Gavazza, S., 2019. Integrating conventional and green roofs for mitigating thermal discomfort and water scarcity in urban areas. *J. Clean. Prod.* 219, 639–648. <https://doi.org/10.1016/j.jclepro.2019.01.068>.
- Georgescu, M., Morefield, P.E., Bierwagen, B.G., Weaver, C.P., 2014. Urban adaptation can roll back warming of emerging megapolitan regions. *Proc. Natl. Acad. Sci. Unit. States Am.* 111 (8), 2909–2914. <https://doi.org/10.1073/pnas.1322280111>.
- Guo, G., Wu, Z., Chen, Y., 2019. Complex mechanisms linking land surface

- temperature to greenspace spatial patterns: evidence from four southeastern Chinese cities. *Sci. Total Environ.* 674, 77–87. <https://doi.org/10.1016/j.scitotenv.2019.03.402>.
- Guo, G., Zhou, X., Wu, Z., Xiao, R., Chen, Y., 2016. Characterizing the impact of urban morphology heterogeneity on land surface temperature in Guangzhou, China. *Environ. Model. Softw.* 84, 427–439. <https://doi.org/10.1016/j.envsoft.2016.06.021>.
- Hamada, S., Ohta, T., 2010. Seasonal variations in the cooling effect of urban green areas on surrounding urban areas. *Urban For. Urban Green.* 9, 15–24. <https://doi.org/10.1016/j.ufug.2009.10.002>.
- Huang, B., Ni, G.H., Grimmond, C.S.B., 2019. Impacts of urban expansion on relatively smaller surrounding cities during heat waves. *Atmosphere* 10 (7), 364. <https://doi.org/10.3390/atmos10070364>.
- Imran, H.M., Kala, J., Ng, A.W.M., Muthukumaran, S., 2018. Effectiveness of green and cool roofs in mitigating urban heat island effects during a heatwave event in the city of Melbourne in southeast Australia. *J. Clean. Prod.* 197, 393–405. <https://doi.org/10.1016/j.jclepro.2018.06.179>.
- Koc, C.B., Osmond, P., Peters, A., 2018. Evaluating the cooling effects of green infrastructure: a systematic review of methods, indicators and data sources. *Sol. Energy* 166, 486–508. <https://doi.org/10.1016/j.solener.2018.03.008>.
- Kohler, M., Kaiser, D., 2019. Evidence of the climate mitigation effect of green roofs—a 20-year weather study on an extensive green roof (EGR) in Northeast Germany. *Buildings* 9 (7), 157. <https://doi.org/10.3390/buildings9070157>.
- Kong, F., Yin, H., James, P., Puttyra, L.R., He, H.S., 2014. Effects of spatial pattern of greenspace on urban cooling in a large metropolitan area of eastern China. *Landscape. Urban Plan.* 128, 35–47. <https://doi.org/10.1016/j.landurbplan.2014.04.018>.
- Li, X.H., Lin, T., Zhang, G.Q., Xiao, L.S., 2011. Dynamic analysis of island urban spatial expansion and its determinants: a case study of Xiamen Island. *J. Geogr. Sci.* 21 (3), 503–520.
- Li, D., Bou-Zeid, E., Oppenheimer, M., 2014. The effectiveness of cool and green roofs as urban heat island mitigation strategies. *Environ. Res. Lett.* 9 (5), 055002. <https://doi.org/10.1088/1748-9326/9/5/055002>.
- Li, D., Liao, W.L., Ridgen, A.J., Liu, X.P., Wang, D.G., Malyshev, S., Shevliakova, E., 2019. Urban heat island: aerodynamics or impermeability? *Sci. Adv.* 5, eaau4299.
- Li, M., Ye, C.D., 2015. Threshold standard and global distribution of high-density cities. *World. Reg. Stud.* 24 (1), 38–45.
- Lin, T., Sun, C., Li, X., Zhao, Q., Zhang, G., Ge, R., Ye, H., Huang, N., Yin, K., 2016. Spatial pattern of urban functional landscapes along an urban–rural gradient: a case study in Xiamen City, China. *Int. J. Appl. Earth Obs. Geoinf.* 46, 22–30. <https://doi.org/10.1016/j.jag.2015.11.014>.
- Luo, H.B., Liu, X., Anderson, B.C., Zhang, K., Li, X., Huang, B., Li, M., Mo, Y., Fan, L.Q., Shen, Q., Chen, F.H., Jiang, M.S., 2015. Carbon sequestration potential of green roofs using mixed-sewage-sludge substrate in Chengdu world modern garden city. *Ecol. Indicat.* 49, 247–259. <https://doi.org/10.1016/j.ecolind.2014.10.016>.
- Maggiotto, G., Buccolieri, R., Santo, M.A., Leo, L.S., Sabatino, S.D., 2014. Validation of temperature-perturbation and CFD-based modelling for the prediction of the thermal urban environment: the Lecce (IT) case study. *Environ. Model. Softw.* 60 (7), 69–83. <https://doi.org/10.1016/j.envsoft.2014.06.001>.
- Markham, B., Barsi, J., Kvaran, G., Ong, L., Kaita, E., Biggar, S., Helder, D., 2014. Landsat-8 operational land imager radiometric calibration and stability. *Remote Sens.* 6, 12275–12308. <https://doi.org/10.3390/rs61212275>.
- Norton, B.A., Coutts, A.M., Livesley, S.J., Harris, R.J., Hunter, A.M., Williams, N.S., 2015. Planning for cooler cities: a framework to prioritise green infrastructure to mitigate high temperatures in urban landscapes. *Landscape. Urban Plan.* 134, 127–138. <https://doi.org/10.1016/j.landurbplan.2014.10.018>.
- Peng, L.H., Jim, C.Y., 2015. Seasonal and diurnal thermal performance of a subtropical extensive green roof: the impacts of background weather parameters. *Sustainability* 7, 11098–11113. <https://doi.org/10.3390/su70811098>.
- Peng, J., Xie, P., Liu, Y.X., Ma, J., 2016. Urban thermal environment dynamics and associated landscape pattern factors: a case study in the Beijing metropolitan region. *Remote Sens. Environ.* 173, 145–155. <https://doi.org/10.1016/j.rse.2015.11.027>.
- Perini, K., Magliocco, A., 2014. Effects of vegetation, urban density, building height, and atmospheric conditions on local temperatures and thermal comfort. *Urban For. Urban Green.* 13 (3), 495–506. <https://doi.org/10.1016/j.ufug.2014.03.003>.
- Qin, N., Ruan, H.M., Man, W., Li, Z.M., Luan, H.J., Sun, F.Q., Li, H., 2018. Spatial-temporal change of land surface temperature landscape patterns in bay city. *J. Fuzhou. Univ.* 46 (5), 657–664.
- Qin, Z., Karnieli, A., Berliner, P., 2001. A mono-window algorithm for retrieving land surface temperature from Landsat TM data and its application to the Israel-Egypt border region. *Intern. J. Remote Sens.* 22, 3719–3746. <https://doi.org/10.1080/01431160010006971>.
- Razzaghmanesh, M., Beecham, S., Salemi, T., 2016. The role of green roofs in mitigating urban heat island effects in the metropolitan area of Adelaide, South Australia. *Urban For. Urban Green.* 15, 89–102. <https://doi.org/10.1016/j.ufug.2015.11.013>.
- Roy, D.P., Wulder, M.A., Loveland, T.R., Woodcock, C.E., Allen, R.G., Anderson, M.C., Scambos, T.A., 2014. Landsat-8: science and product vision for terrestrial global change research. *Remote Sens. Environ.* 145, 154–172. <https://doi.org/10.1016/j.rse.2014.02.001>.
- Sailor, D.J., Elley, T.B., Gibson, M., 2012. Exploring the building energy impacts of green roof design decisions—a modeling study of buildings in four distinct climates. *J. Build. Phys.* 35 (4), 372–391. <https://doi.org/10.1177/174425911420076>.
- Sangkakool, T., Techato, K., Zaman, R., Brudermann, T., 2018. Prospects of green roofs in urban Thailand - a multi-criteria decision analysis. *J. Clean. Prod.* 196, 400–410. <https://doi.org/10.1016/j.jclepro.2018.06.060>.
- Santamouris, M., 2013. Using cool pavements as a mitigation strategy to fight urban heat island- A review of the actual developments. *Renew. Sustain. Energy Rev.* 26, 224–240. <https://doi.org/10.1016/j.rser.2013.05.047>.
- Santamouris, M., 2014. Cooling the cities: a review of reflective and green roof mitigation technologies to fight heat island and improve comfort in urban environments. *Sol. Energy* 103, 682–703. <https://doi.org/10.1016/j.solener.2012.07.003>.
- Santamouris, M., Cartalis, C., Synnefa, A., Kolokotsa, D., 2015. On the impact of urban heat island and global warming on the power demand and electricity consumption of buildings: a review. *Energy Build.* 98, 119–124. <https://doi.org/10.1016/j.enbuild.2014.09.052>.
- Santos, T., Tenedório, J., Gonçalves, J., 2016. Quantifying the city's green area potential gain using remote sensing data. *Sustainability* 8, 1247. <https://doi.org/10.3390/su8121247>.
- Sharma, A., Conry, P., Fernando, H.J.S., Alan, F.H., Hellmann, J.J., Chen, F., 2016. Green and cool roofs to mitigate urban heat island effects in the Chicago metropolitan area: evaluation with a regional climate model. *Environ. Res. Lett.* 11 (6), 064004. <https://doi.org/10.1088/1748-9326/11/6/064004>.
- Sharma, A., Fernando, H.J., Hamlet, A.F., Hellmann, J.J., Barlage, M., Chen, F., 2017. Urban meteorological modeling using WRF: a sensitivity study. *Int. J. Climatol.* 37, 1885–1900. <https://doi.org/10.1002/joc.4819>.
- Shen, Y.J., Wang, C.G., Cao, L., Gao, H.Y., Wang, Y.W., 2017. A case study of simulated cooling effect of roof greening in urban area of Nanjing. *Meteorol. Mon.* 43 (5), 610–619.
- Skelhorn, C., Lindley, S., Levermore, G., 2014. The impact of vegetation types on air and surface temperatures in a temperate city: a fine scale assessment in Manchester, UK. *Landscape. Urban Plan.* 121, 129–140. <https://doi.org/10.1016/j.landurbplan.2013.09.012>.
- Smith, K.R., Roebber, P.J., 2011. Green roof mitigation potential for a proxy future climate scenario in Chicago, Illinois. *J. Appl. Meteorol. Climatol.* 50, 507–522. <https://doi.org/10.1175/2010JAMC23371>.
- Sung, H., Oh, J.T., 2011. Transit-oriented development in a high-density city: identifying its association with transit ridership in Seoul, Korea. *Cities* 28, 70–82. <https://doi.org/10.1016/j.cities.2010.09.004>.
- Sun, R., Lü, Y., Chen, L., Yang, L., Chen, A., 2013. Assessing the stability of annual temperatures for different urban functional zones. *Build. Environ.* 65, 90–98. <https://doi.org/10.1016/j.buildenv.2013.04.001>.
- Teotónio, I., Silva, C.M., Cruz, C.O., 2018. Eco-solutions for urban environments regeneration: the economic value of green roofs. *J. Clean. Prod.* 199, 121–135. <https://doi.org/10.1016/j.jclepro.2018.07.084>.
- Tewari, M., Yang, J., Kusaka, H., Salamanca, F., Weston, C., Treinish, L., 2019. Interaction of urban heat islands and heat waves under current and future climate conditions and their mitigation using green and cool roofs in New York City and Phoenix, Arizona. *Environ. Res. Lett.* 14, 034002. <https://doi.org/10.1088/1748-9326/aa4f43>.
- Voogt, J.A., Oke, T.R., 2003. Thermal remote sensing of urban climates. *Remote Sens. Environ.* 86 (3), 370–384. [https://doi.org/10.1016/S0034-4257\(03\)00079-8](https://doi.org/10.1016/S0034-4257(03)00079-8).
- White, M.A., Nemani, R.R., Thornton, P.E., Running, S.W., 2002. Satellite evidence of phenological differences between urbanized and rural areas of the eastern United States deciduous broadleaf forest. *Ecosystems* 5, 260–273. <https://doi.org/10.1007/s10021-001-0070-8>.
- Yang, J., Bou-Zeid, E., 2019. Scale dependence of the benefits and efficiency of green and cool roofs. *Landscape. Urban Plan.* 185, 127–140. <https://doi.org/10.1016/j.landurbplan.2019.02.004>.
- Yang, J., Wang, Z.-H., 2017. Planning for a sustainable desert city: the potential water buffering capacity of urban green infrastructure. *Landscape. Urban Plan.* 167, 339–347. <https://doi.org/10.1016/j.landurbplan.2017.07.014>.
- Yang, J., Wang, Z.-H., Kaloush, K.E., 2015. Environmental impacts of reflective materials: is high albedo a ‘silver bullet’ for mitigating urban heat island? *Renew. Sustain. Energy Rev.* 47, 830–843. <https://doi.org/10.1016/j.rser.2015.03.092>.
- Zhang, B., Xie, P., Gao, J.X., Yang, Y., 2014. The cooling effect of urban green spaces as a contribution to energy-saving and emission-reduction: a case study in Beijing, China. *Build. Environ.* 76, 37–43. <https://doi.org/10.1016/j.buildenv.2014.03.003>.
- Zhou, Q., 2014. A review of sustainable urban drainage systems considering the climate change and urbanization impacts. *Water* 6, 976–992. <https://doi.org/10.3390/w6040976>.
- Zhou, W., Wang, J., Cadenasso, M.L., 2017. Effects of the spatial configuration of trees on urban heat mitigation: a comparative study. *Remote Sens. Environ.* 195, 1–12. <https://doi.org/10.1016/j.rse.2017.03.043>.
- Zinzi, M., Agnoli, S., 2012. Cool and green roofs. An energy and comfort comparison between passive cooling and mitigation urban heat island techniques for residential buildings in the Mediterranean region. *Energy Build.* 55, 66–76. <https://doi.org/10.1016/j.enbuild.2011.09.024>.
- Zribi, M., Le Hégarat-Mascle, S., Taconet, O., Ciarletti, V., Vidal-Madjar, D., Boussema, M.R., 2003. Derivation of wild vegetation cover density in semi-arid regions: ERS2/SAR evaluation. *Int. J. Remote Sens.* 24 (6), 1335–1352. <https://doi.org/10.1080/0143116021046668>.